

Luminous early-type field galaxies at $z \sim 0.4$ – I. Observations and redshift catalogue of 581 galaxies

J.P. Willis,^{1*} P.C. Hewett¹ and S.J. Warren²

¹*Institute of Astronomy, Madingley Road, Cambridge CB3 0HA*

²*Blackett Laboratory, Imperial College of Science Technology and Medicine, Prince Consort Road, London SW7 2BZ*

Accepted 2001 March 15. Received 2001 February 27; in original form 2000 October 21

ABSTRACT

We have compiled a sample of ~ 9600 bright, $i \leq 18.95$, red, $b_j - r > 2$, candidate galaxies in an area of 220 deg^2 . These are luminous, $L > L^*$, field early-type galaxies with redshifts $0.3 \lesssim z \lesssim 0.6$. We present a redshift catalogue of a sub-sample of 581 targets. The galaxies were selected according to their broadband $b_j r i$ colours from United Kingdom Schmidt Telescope plates, and have a surface density on the sky of only $\sim 50 \text{ deg}^{-2}$. Such luminous field galaxies are virtually absent from published redshift surveys and the catalogue provides a large sample of the most luminous normal galaxies, at cosmological distances. The statistical properties of the galaxy spectra, including absorption line and emission line measures, are presented and a composite spectrum constructed. The nature of the sample, combined with the relatively bright apparent magnitudes make the galaxies suitable targets for several key investigations in galaxy evolution and cosmology.

Key words: early-type galaxies – photometry: spectroscopy.

1 INTRODUCTION

Systematic galaxy redshift surveys to faint magnitude limits have produced a wealth of information relating to the luminosity function and evolution of the bulk of the galaxy population out to redshifts of $z \sim 1$ (Ellis 1997). Such studies have been complemented by targeted investigations of rich clusters of galaxies out to a comparable redshift (e.g. van Dokkum et al. 1998). Given the prevalence of luminous ($L \gtrsim L^*$) early-type galaxies within rich clusters it has proved possible to obtain high-quality data for a large sample of such galaxies in rich clusters. By contrast, while the majority of luminous early-type galaxies are located in field regions, where “field” is taken to indicate environments outside of rich galaxy clusters, existing redshift surveys contain few examples of field early-type galaxies with luminosities in excess of L^* at redshifts $0.2 \leq z \leq 0.8$. Although such galaxies are intrinsically luminous, and hence possess relatively bright apparent magnitudes, their very low volume density leads to a surface density on the sky of only $\sim 100 \text{ deg}^{-2}$. Deep redshift surveys, employing flux limits at R -band or longer wavelengths, cover too small an area of sky to include more than a few such objects. For example, only one of the 591 galaxies in the CFRS survey with

spectroscopic identifications (Crampton et al. 1995) has a redshift $0.3 \leq z \leq 0.6$ and is bright enough for inclusion in the sample presented here. Wide field surveys, such as the 2dF Redshift Survey (Colless 1999), cover sufficient area but the associated flux limits, often in a blue passband, are bright. The integrated spectrum of an old passively evolving stellar population exhibits a strong depression of the continuum shortward of 4000 \AA resulting in a large k -correction for blue passbands at redshifts $z \gtrsim 0.25$, giving observed colours $B - R > 2$. The brighter galaxies in the sample presented here possess blue apparent magnitudes, $B \sim 21$, that are still too faint by a magnitude or more for inclusion in the 2dF Redshift Survey. Thus, notwithstanding the pioneering work of Hamilton (1985) in identifying early-type galaxies at cosmological redshifts, no large samples of the most luminous field early-type galaxies at significant redshifts $z \sim 0.4$ exist.

The motivation for compiling a well-defined sample of luminous early-type galaxies at redshift $z \sim 0.4$ is considerable, offering the prospect of undertaking a number of projects not possible hitherto. Examples include: i) a survey for strong gravitational lensing based on a study of the optimal deflector population (Hewett et al. 2000), ii) investigating the Fundamental Plane for luminous galaxies as a function of environment at a significant lookback time, iii) establishing the evolution of the space density and luminosity function of the most massive galaxies, and iv) quantifying the evolution of galaxy clustering on large scales. Papers de-

* Present address: Departamento de Astronomía y Astrofísica, P. Universidad Católica, Avenida Vicuña Mackenna 4860, Casilla 306, Santiago 22, Chile

scribing the results of such investigations are in preparation and in this first paper of the series we describe the procedures used to identify luminous field galaxies with redshifts $0.3 \leq z \leq 0.6$ and present an initial spectroscopic catalogue of 581 galaxies.

In Section 2 we describe the compilation of a sample of ~ 9600 bright, red galaxies, $i \leq 18.95$, $b_j - or > 2$, over 220 deg^2 , from scans of United Kingdom Schmidt Telescope photographic plates. Multifibre spectroscopic observations, using the 2dF instrument on the Anglo Australian Telescope, of 581 of these candidate luminous early-type galaxies are presented in Section 3. The section includes a discussion of the reduction procedures employed to extract the galaxy spectra, which are relatively faint by the standards of many observations made with the instrument to date. The global properties of the galaxy sample are investigated in Section 4. The redshift distribution and number magnitude counts are presented and a composite spectrum constructed. The absorption and emission line properties of the galaxies are reviewed and the prevalence of [OII] 3727 emission quantified. Further details of the absorption line strength measurements are presented in the Appendix. The paper concludes with a summary of the properties of the galaxy sample in Section 5.

2 GALAXY SELECTION AND PHOTOMETRIC CALIBRATION

This programme grew out of an earlier survey for high-redshift $z > 2.2$ quasars (Warren et al. 1991), and the observational material and data processing for the two surveys are very similar. Early-type galaxies of redshift $z \sim 0.4$ and quasars of $z \sim 4$ have similar $B - R$, $R - I$ colours, and the quasar samples were contaminated by galaxies. The two populations may be distinguished on the basis of image profile since the galaxies are extended and are marginally resolved on the plates. Numerically the galaxies overwhelm the quasars, so for the quasar survey it was essential to optimise the separation of resolved and unresolved sources.

2.1 Compilation of the b_j , or , i multicolour dataset

Relative to Galactic stars, early-type galaxies of redshift $z \sim 0.4$ appear to be very red in $B - R$ but neutral in $R - I$, and may be selected by identifying objects that lie to the red in $B - R$ of the locus of early M-stars in a BRI two-colour diagram. We have compiled a sample of 9599 bright, $i \leq 18.95$, red galaxies, over 220.0 deg^2 . The basic photometric data used were the uncalibrated raw object catalogues produced by Automated Plate Measuring (APM) machine scans of photographic plates obtained at the United Kingdom Schmidt Telescope (UKST). The survey covers seven UKST fields, listed in Table 1. A scan of a single UKST field covers 33 deg^2 and the plates scanned are listed in Table 2. The UKST passbands are defined by emulsion and filter combinations. For the blue, red, and near-infrared the combinations IIIa-J+GG395, IIIa-F+RG590, and IV-N+RG715 define the b_j , or , and i bands respectively (we use lower case for the UKST photometric system). In field F833 we used the narrower r band, defined by IIIa-F+RG630, as there were no suitable or plates. All magnitudes are quoted

Table 1. UKST field centre coordinates.

Field	RA (hh:mm)	Dec. (dd:mm)	(B1950.0)
SGP	00:53	-28:08	
F297	01:44	-40:00	
F833	03:20	+00:00	
F855	10:40	+00:00	
F864	13:40	+00:00	
MT	22:03	-18:54	
F345	22:06	-40:00	

Table 2. UKST photographic plate numbers and galaxy magnitude limits for each field.

Field	$b_j(1)$	$b_j(2)$	$r(1)$	$r(2)$	$i(1)$	$i(2)$
SGP	21.99	22.35	20.91	20.55	19.58	19.14
SGP	J9766	J9771	OR9563	OR9595	I12092	I12198
F297	22.17	21.49	20.37	20.62	19.30	19.33
F297	J3593	J15720	OR10353	OR10462	I10435	I10441
F833	22.29	21.99	20.66	20.36	20.09	19.79
F833	J9752	J14606	R11438	R11573	I11437	I16828
F855	22.18	21.97	20.94	20.74	19.08	19.17
F855	J9309	J16076	OR10854	OR14220	I6910	I10873
F864	22.23	22.02	20.21	20.46	19.01	18.84
F864	J9108	J11701	R6808	OR13041	I10141	I12562
MT	22.23	22.24	20.34	20.48	18.89	19.28
MT	J12032	J12129	OR11946	OR12094	I6389	I7058
F345	22.52	22.40	20.66	20.64	19.18	19.90
F345	J2656	J3585	OR12611	OR13849	I11430	I12727

in the natural system defined by the UKST passbands, zero-pointed to the standard Johnson/Cousins system.

The APM catalogues contain information on the brightness, shape, and surface brightness profile of the objects detected, while the APM instrumental magnitudes are related to standard magnitudes by a calibration that is approximately linear, with a slope close to -1.0 , and a zero-point that is different for each plate. The steps involved to produce clean calibrated multicolour data sets from the raw catalogues are described in detail by Warren et al. (1991). For brevity, therefore, only an outline of the data processing is provided here, except where the procedure differed between the new galaxy survey and the earlier quasar survey.

The multicolour object catalogues are defined by objects that are detected on both the red plates. The magnitudes were averaged after transforming the instrumental magnitudes from one red plate to the reference red plate. Then a search was made for these objects on the plates of the other passbands, averaging the magnitude if detected on both plates of a particular passband. If the object was undetected on either plate the detection limit on the deeper plate was recorded. The photometric errors, as a function of magnitude, were established through an analysis of the scatter in the difference between magnitudes of all the objects detected on the two plates of the same passband. Fitting a polynomial function to this distribution provided a magnitude error for each object, detected on each plate. The red plates are sufficiently deep that all candidate early-type galaxies satisfying the i -magnitude and colour cuts used to define the galaxy sample are detected.

The objects in the raw catalogues are classified as stellar or non-stellar on the basis of a parameter computed from the surface-brightness profile. This classification parameter

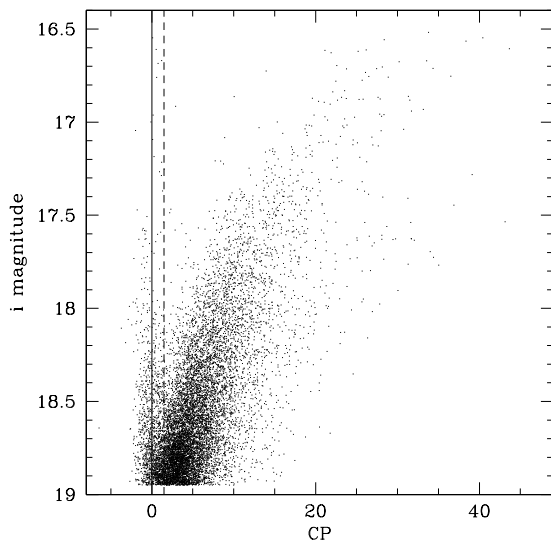


Figure 1. Classification parameter (CP) versus i magnitude. The solid line indicates the stellar locus defined to be $CP = 0$ and the dashed line indicates the applied $CP > 1.5$ selection threshold. Galaxian objects display a trend of greater CP values at brighter apparent magnitudes.

(CP) is rescaled by plotting the parameter against instrumental magnitude, identifying the domain occupied by stars, zeroing to the peak, and normalising by the standard deviation σ , such that for each object on each plate CP now measures how many σ the object lies from the peak. The majority of the galaxies that are the target of this work have half-light radii of order $1''$, and are difficult to distinguish from stars on an individual plate. By averaging the values of CP on all the plates on which an object was detected the separation of stellar and non-stellar objects was greatly improved (Figure 1).

A particular problem for the quasar survey was objects with incorrect photometry, resulting in unusual (and therefore apparently interesting) colours. The most common cause is two objects appearing merged into a single object in one passband pairing with one of the separate objects in another passband. To identify and eliminate such cases we used two parameters; the positional offset between matched objects on different plates, and the object ellipticity. By plotting the distribution of these quantities against instrumental magnitude, outliers were identified and eliminated. This procedure is appropriate for stellar objects, but galaxies which have been matched correctly might be eliminated by the ellipticity criterion. In fact this is less of a problem for our targets because a) at these relatively faint magnitudes the object ellipticity distribution is broader and the cutoff therefore less strict, b) the galaxies have small angular sizes due to their large distances and they appear close to circular due to the seeing, and c) there are very few early-type galaxies with intrinsic ellipticity greater than 0.6. To make this conclusion more quantitative we reran the entire catalogue pipeline for one of our fields, but without the ellipticity cut, and found that in the colour region of interest the number of galaxies decreased by only 1%. We conclude

that the fraction of the total galaxy sample eliminated by the ellipticity cut is negligible.

For the earlier quasar survey, that used 12 plates in each field, we established that about 20% of real sources were removed by the procedures designed to eliminate objects with incorrect photometry (e.g. object mergers, emulsion flaws and satellite trails). Assuming that the incidence of objects with incorrect photometry is consistent across all plates then for the current galaxy survey, which uses only six plates per field, we calculate that $\sim 10\%$ of real sources are lost in this way. The effective area of the survey is therefore reduced from 220.0 deg^2 to 198.0 deg^2 .

At this point the catalogue comprises all cleanly matching objects detected on both the red plates, with APM magnitudes, or limits, in the three bands, as well as photometric errors and an average value of CP. The object x - y positions in the APM catalogues are transformed to celestial J2000.0 coordinates via a plate-solution based on the right ascension, declination and proper motions of the ~ 600 TYCHO-2 catalogue stars (Høg et al. 2000) present on each plate. The root-mean-square positional differences between the catalogued TYCHO-2 star positions and the APM-positions is $\simeq 0.25$ arcsec. Systematic errors in positions, relative to the frame defined by the TYCHO-2 stars, are $\lesssim 0.5$ arcsec across a full UKST field.

2.2 Photometric calibration

Photometric calibration of galaxies on photographic plates is complicated. This is because APM instrumental magnitudes are essentially isophotal magnitudes, but calibrated aperture or total magnitudes are required. The difference between APM isophotal magnitude and aperture magnitude depends on the surface brightness profile of the galaxy, and this inevitably introduces scatter into the calibration, in addition to the photometric errors. In other words the χ^2 for the fit of the calibration-curve will be large. The problem is severe when using a calibration sequence containing all galaxy types, as for example in the APM galaxy survey (Maddox, Efstathiou & Sutherland 1990). The problem is much less severe when calibrating a homogeneous population using CCD measurements of galaxies drawn from the population, as is the case here. Considering this question in more detail, for the population of giant early-type galaxies there is a strong correlation between physical size (e.g. half-light radius) and luminosity. Because the redshift distribution of the sample is quite narrow (Figure 17), this results in a strong (anti-)correlation between size and apparent magnitude. Therefore the magnitude correction from isophotal to aperture magnitude is also strongly correlated with apparent magnitude. Consequently the increased scatter in the calibration curve, due to the spread in magnitude correction at any apparent magnitude, is small. This conclusion is borne out by the measured χ^2 for our calibration curves, and we conclude that the aperture magnitudes are quite reliable.

We obtained CCD images of galaxies in five fields in 1993 November at the Danish 1.5m and ESO 3.6m telescopes on La Silla. Integration times of 1500s, 300s and 240s were used for the B , R , and I bands respectively for the 1.5m, and 300s, 180s and 180s for the 3.6m. CCD images in fields F855 and F864 were obtained in 1997 April

with the 2.5m Isaac Newton Telescope on La Palma. Integration times were 1400 s, 400 s and 400 s for the B , R , and I bands respectively. An average of 23 galaxies (range 12 to 46) were observed in each field. Standard procedures for data reduction were followed in processing these data. Magnitudes were measured using an $8''$ diameter aperture. To convert the Johnson/Cousins magnitudes to UKST magnitudes requires colour equations suitable for the objects in question. For this purpose we computed synthetic colours of early-type galaxies in the redshift range $0.3 \leq z \leq 0.6$, obtaining the following linear fits for the colour terms:

$$b_j - B = 1.233 - 0.593(B - R)$$

$$or - R = -0.307 + 0.337(R - I)$$

$$r - R = -0.212 + 0.056(R - I)$$

$$i - I = 0.0$$

The galaxy CCD magnitudes were transformed to the UKST natural system, and a least-squares linear calibration solution derived. Typical errors for the standards were 0.08, 0.02, 0.03 mag in B , R , I respectively, and 0.13, 0.06, 0.12 for the photographic magnitudes. A weighted linear solution was computed, assuming errors dominated by the photographic magnitudes, providing a satisfactory fit over the limited magnitude range of the sample. A correction for Galactic reddening of $E(B - V) = 0.05$ mag was made for F833 which has a Galactic latitude $b \sim -45^\circ$. Using this calibration the number of galaxies meeting the colour selection criteria showed rather large variations from field to field. Therefore, for fields with few galaxy standards we permitted small adjustments to the calibration zero-points, of ≤ 0.1 mag. Adjustments were determined by a careful comparison of the mean galaxy colours, and the surface density of the colour-selected galaxy samples. The accuracy of the adopted zero-point in each field is thus $\simeq \pm 0.05$ mag.

2.3 Sample selection

Early-type galaxies are selected according to the CP value and location in $b_j ori$ colour space. Colour-selection on the $b_j - or$ versus $or - i$ colour plane is a highly effective method of isolating early-type galaxies from both stars and later galaxy types. The locus occupied by early-type galaxies is largely determined by the effect of the 4000\AA break moving through the b_j passband with increasing redshift. Figure 2 shows the locus defined by an evolving early-type galaxy spectral energy distribution (Pozzetti et al. 1996). The locus defined by an evolving Sab spiral galaxy spectral energy distribution (Pozzetti et al. 1996) is shown for comparison. Each locus was created by specifying a redshift of galaxy formation $z_{form} = 4.5$ and a cosmological model described by the parameters $\Omega_M = 0.3$, $\Omega_\Lambda = 0.7$ and $H_0 = 70 \text{ km s}^{-1} \text{ Mpc}^{-1}$. Dispersion about the locus arises from random photometric errors and intrinsic colour variation within the galaxy population. Defining the multi-colour parameter space listed in Table 3 isolates early-type galaxies in the redshift interval $0.3 \lesssim z \lesssim 0.55$. A random error $\gtrsim 5\sigma$ in the measurement of early-type spiral colours is necessary to scatter such galaxies into the region defined by the colour-selection criteria. The locus of stellar colours on the $b_j - or$ versus $or - i$ plane is defined by the main sequence and

Table 3. Photometric selection criteria.

16.5	<	m_i	<	18.95
2.15	<	$b_j - or$	<	3.00
		$or - i$	<	1.05
2.95	<	$b_j - i$		

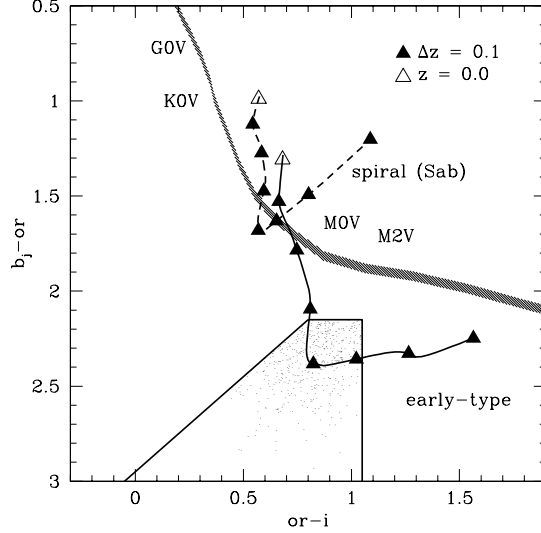


Figure 2. $b_j ori$ two-colour diagram indicating the relative position of loci representing evolving early-type galaxies (solid curve) and spiral galaxies (dashed curve) versus redshift (see text for additional details), and the stellar main sequence (shaded region). The boundaries employed to select early-type galaxy candidates are shown by the solid polygon at the lower-middle of the plot. Individual candidate galaxy colours are indicated by small dots.

falls outside the defined colour selection region. However, dispersion about the locus could lead to contamination of the early-type galaxy sample by M-type stars. The stellar main sequence is sufficiently removed from the nearest colour-selection boundary that contamination of the early-type galaxy sample is likely to be low. Furthermore, the requirement that candidate galaxies possess a morphological classification $CP > 1.5$ further reduces the potential stellar contamination. The effectiveness of the morphological selection is addressed in Section 3.4, where the results of spectroscopic observations of a sample of objects satisfying the colour-selection criteria but possessing morphological classifications $CP < 1.5$ are presented.

The selection procedure as described above was applied to the seven UKST fields, identifying 9599 early-type galaxy candidates from an effective area of 198.0 deg^2 . The surface density of objects at the faint magnitude limit ($m_i \leq 18.95$) is $\sim 50 \text{ deg}^{-2}$. Figure 3 shows the i -band number-apparent magnitude relation for the sample.

3 SPECTROSCOPY

3.1 Observations

Spectroscopic observations were performed using the Two-degree Field (2dF) multi-fibre spectrograph at the Anglo-Australian Telescope (AAT). With a surface density of

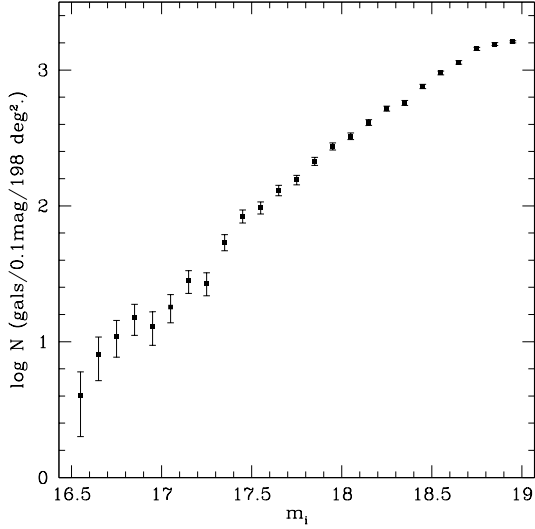


Figure 3. Number–apparent magnitude distribution for early-type galaxy candidates in the seven UKST fields. Poisson error bars are shown.

Table 4. Spectroscopic observations.

Date	Field	Exposure time (s)	N_{spectra}
98/09/16–17	F297, MT	12,600	485
98/05/03	F864	6,300	18
97/07/31	F864	7,200	78

$\sim 50 \text{ deg}^{-2}$ up to 150 candidate galaxies can be observed simultaneously with 2dF. In addition to observations of early-type galaxy candidates, a sample of 33 stellar candidates (i.e. objects satisfying the colour criteria but with $\text{CP} < 1.5$) were included in the 1998 September 16–17 2dF observations in order to determine directly the level of incompleteness in the early-type galaxy sample.

Target 2dF fields were configured using the observatory supplied software package `configure` (Bailey and Glazebrook 1999) which automatically allocates fibre positions to guide star, early-type galaxy and stellar targets. Sky fibres were allocated according to the automated `skygrid` procedure within `configure`. Sky fibres were allocated in excess of the conventional rate (Wyse and Gilmore 1992) as previous experience with 2dF observations indicated that systematic instrumental effects (spectrograph focus, scattered light) rather than photon noise, limit the accuracy of sky-subtraction.

The spectrograph configuration was essentially identical for all the observing runs, employing the AAO 600V gratings to give spectra covering the wavelength range $4600 - 6800 \text{ \AA}$ with a resolution of $\sim 4 \text{ \AA}$. Observations of each target field were made up of individual exposures of $1800 - 2100 \text{ s}$. Tungsten-lamp flat-field exposures and several CuHe+CuAr arc calibration exposures were taken for each target field. Offset sky exposures were also obtained but were not in fact used in the reductions. A summary of the spectroscopic observations are given in Table 4. The spectra presented in Section 4 were obtained from observations made over the two-nights of 1998 September 16–17 (Table 5). Atmospheric transparency was good throughout and the

seeing varied between $1''.5$ and $2''.0$. Aside from some contaminating light from an uncovered Light Emitting Diode affecting spectrograph B in exposures obtained for one field (see next sub-Section) no significant problems occurred with the telescope or the 2dF instrument. The discussion of the reductions and the analysis of the spectroscopic properties of the galaxy sample presented in subsequent sections is based on the data obtained during this run.

Observations made prior to the 1998 September run were obtained with the 2dF instrument still not fully commissioned and the weather in all cases produced periods of variable transparency. As a result only some of the exposures obtained were of use and spectra were obtained for only a subset of the targets. However, the spectra of a significant number of galaxies observed were of sufficient quality to yield reliable redshifts. These spectra were not included in the sample employed for statistical analysis but the positions, magnitudes and redshifts of the galaxies are included in Table 8.

3.2 2dF data reduction

Spectra were reduced using the AAO-supplied `2dFdr` package and standard `IRAF`[†] routines. All spectra were inspected visually prior to applying reduction techniques. Contaminating light from an uncovered Light Emitting Diode (LED) affecting spectrograph B (CCD2) was noted in exposures obtained for one field (MTF5). The contaminating signal includes a broad ($\sim 1000 \text{ \AA}$) emission feature located at $\sim 6000 \text{ \AA}$. The effect of this contamination on the reduction methods is discussed in subsequent sections. Spectra were de-biased, scattered light subtracted, extracted and wavelength calibrated using the `2dFdr` package. Correction of fibres to a uniform transmission level and sky-subtraction were performed using specially written routines in the `IRAF` environment.

3.3 Sky-subtraction

The signal received through a 2dF fibre from a galaxy target is a factor ~ 3 fainter than the R -band night-sky. Accurate determination of relative fibre transmission levels and subtraction of the night-sky contribution are essential to produce high quality object spectra. The sky conditions were stable over the observations of individual fields. As the spectrograph exhibited a high degree of stability, with wavelength shifts over the observation of individual fields corresponding to considerably less than one CCD-pixel, the individual exposures of each target field were combined prior to correction for fibre transmission and sky-subtraction. Spectra were co-added within `2dFdr` applying a 5σ -clipping rejection criterion to remove cosmic ray events.

Relative fibre transmission levels were estimated by combining the emission-line signal in prominent night-sky emission-lines located at 5577 \AA , 5890 \AA and 6300 \AA for each object+sky and sky fibre (Lissandrini, Cristiani and La

[†] IRAF is distributed by the National Optical Astronomy Observatories, which are operated by the Association of Universities for Research in Astronomy, Inc., under cooperative agreement with the National Science Foundation.

Table 5. 2dF Field coordinates and target classifications for 1998/09/16–17 observations.

Field	Centre (J2000)		Early-type	Fibre allocations			
	RA (hh:mm:ss.s)	dec. (dd:mm:ss)		Stellar	QSO	Sky	Parked
MTF 2	22:11:58.3	-20:33:07	141	8	74	102	75
MTF 5	21:56:27.2	-20:47:20	114	17	75	108	87
F297 1	01:45:59.2	-39:51:34	135	4	0	200	61
F297 2	01:35:15.6	-40:05:10	135	4	0	208	43

Franca 1994). The “continuum” contribution from the sky and object in each fibre spectrum was removed by fitting and subtracting a 21st order cubic spline function. The narrow absorption features in early-type galaxy spectra are not strong enough to bias significantly the estimate of the night-sky emission signal. Use of the night-sky emission line strength method is relatively unaffected by uncertainties in the scattered light correction applied to the frames and offers a significant advantage over the use of offset sky exposures to estimate the relative fibre transmissions. Employing a relatively wide ($\sim 50 \text{ \AA}$) window to calculate the signal associated from night-sky emission lines minimises systematic variation of the line-to-continuum ratio caused by varying spectrograph focus. The standard 2dFdr method (option SKYLINE) was found to be susceptible to this effect. Individual fibre spectra were then corrected to a uniform transmission level.

Variations in spectrograph focus along the slit ($\sim 20\%$ from the centre to the edge of particular fields) and hence with fibre number, limit the effectiveness of a sky-subtraction method based upon a single template sky spectrum. Therefore, a sky-spectrum template was formed from ~ 20 sky-fibre spectra with the best focus on each combined exposure. The resulting template sky-spectrum was then convolved with a Gaussian profile of varying width, chosen to match the observed Full-Width Half-Maximum (FWHM) of prominent night-sky emission-lines in each individual object+sky- and sky-fibre spectra.

The effectiveness of the fibre-transmission and sky-subtraction procedures compared to the standard 2dFdr reduction is illustrated in Figure 4 and Figure 5. The systematic trends in residual zero-point level following sky-subtraction are much reduced and individual examples of poor sky-subtraction can show dramatic improvements. The accuracy of sky-subtraction, calculated from the dispersion in the zero-point of sky-subtracted sky-fibres relative to the mean in a given frame, is $\pm 2\%$. The dispersion is significantly larger than the theoretical Poisson limit, $< 1\%$, but represents a significant improvement over that achieved, $\sim 3 - 5\%$, through employing the default reduction procedures in 2dFdr.

3.4 Spectral classification

At this point the 2dF spectra consist of wavelength calibrated one-dimensional sky-subtracted spectra, each of which has an associated classification (“galaxy”, “stellar”, “sky”) derived from the input catalogue.

3.4.1 Stellar candidates

Comparison of each of the spectra of the 33 stellar targets to reference spectra of cool main-sequence stars (Turnshek

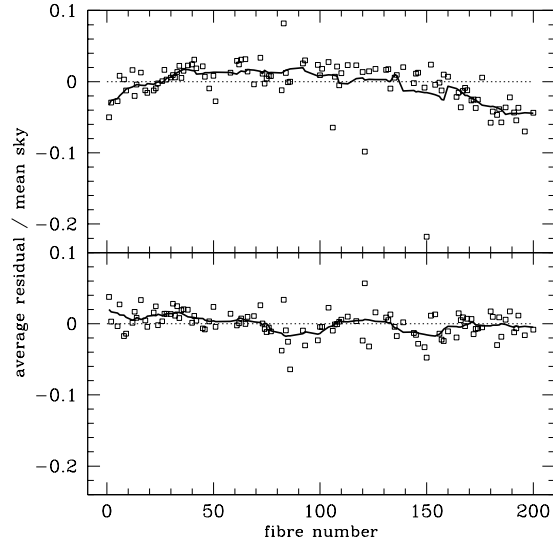


Figure 4. Top panel: average residual for 2dFdr sky-subtracted sky-fibres in Field F297 2 CCD2 (observed on 1998/09/17). The solid line is obtained by median filtering the data over an 11-fibre window. The dotted line indicates zero residual. Bottom panel: average residual per pixel obtained using the modified sky-subtraction procedure described in the text. The rms deviation about the zero level is equivalent to a $\pm 2\%$ sky-subtraction uncertainty.

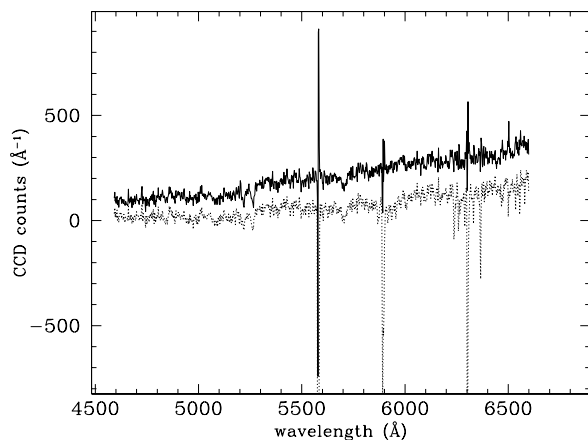


Figure 5. Example of an early-type galaxy spectrum (solid line) reduced using the modified sky-subtraction procedure compared to the spectrum of the same object reduced using the standard 2dFdr sky-subtraction method (dotted line).

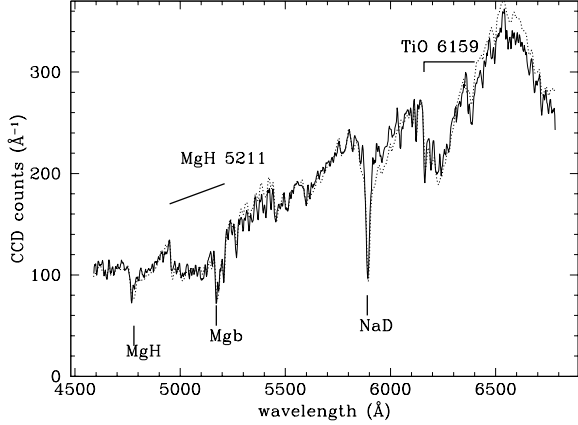


Figure 6. Mean stellar spectrum (solid line) generated from 33 individual response function corrected spectra (see Section 3.6) compared to a template M2V spectrum from the atlas of Pickles (1998) (dotted line). Strong absorption features are indicated.

et al. 1985) produced unambiguous identifications as late K and early M stars. Individual spectra showed evidence for some, or all, of broad molecular absorption bands, such as TiO, and narrow absorption lines (MgH4780, Mgb, NaD and CaH) superimposed upon a characteristic continuum shape. The sample of stellar candidates does not contain any galaxies, showing that the incompleteness in the early-type galaxy sample due to misclassification of galaxies as stars is extremely small.

A composite spectrum was generated from the stellar spectra. Spectra were combined using inverse-variance weighting and 3σ -clipping rejection criteria to remove individual pixels affected by residual cosmic rays and night-sky emission lines. Strong residual signatures associated with the very strong night-sky emission-lines at 5577Å, 5890Å, 6300Å and 6360Å were replaced by a local median-filtered continuum estimate. Figure 6 indicates that the composite spectrum corrected for the instrumental response (Section 3.6) closely resembles a star of type M2V (Turnshek et al. 1985; Pickles 1998).

3.4.2 Galaxy candidates

Classification of the spectra of candidate galaxies was accomplished via cross-correlation with representative early-type galaxy and stellar templates. A high signal-to-noise ratio (S/N) early-type galaxy spectral energy distribution (SED) derived from observations of local early-type galaxies (Kinney et al. 1996) and the composite stellar spectrum derived above were employed as templates. The residual signature of strong night-sky emission-lines in the object spectra were excluded from the cross-correlation analysis to avoid introducing spurious signals. Individual spectra were cross-correlated with each template using the IRAF routine `xciao` (Tonry and Davis 1979). This routine effectively removes continuum shape information extending over large wavelength intervals and calculates the cross-correlation signal between continuum discontinuities and absorption and emission features in the spectra. The cross-correlation can be performed over a range of radial velocities in order to ascer-

Table 6. Classification of candidate early-type galaxy spectra in the 1998/09/16–17 sample.

Early-type galaxy	485
Stellar	8
Unclassified (low S/N)	24
Unclassified (LED/defect)	8
Total	525

tain the radial velocity (redshift) for the template that maximises the cross-correlation signal. Cross-correlation with the stellar template was performed over the radial velocity interval $\pm 500 \text{ km s}^{-1}$. Cross-correlation with the galaxy template was performed over the radial velocity interval $0 - 200000 \text{ km s}^{-1}$ to allow for early-type galaxy redshifts $z \leq 0.67$ (exceeding the maximum anticipated redshift).

Figure 7 displays the resulting R-value[‡] for each template applied to each spectrum from the 1998/09/16–17 observations. Stellar spectra lie below $R_{\text{galaxy}} = 3.5$ and, for $R_{\text{star}} > 3.5$, are clearly separated from candidate early-type galaxy spectra. This leaves a potential zone of confusion containing 126 spectra with $R_{\text{star}} \lesssim 3.5$ and $R_{\text{galaxy}} \lesssim 3.5$. Although these spectra generally display low-S/N, spectral information can still be used to discriminate between galaxies and stars. Candidate early-type galaxy spectra were classified visually by identifying CaII(H+K), G-band, Mgb and Balmer absorption observed at $0.25 \lesssim z \lesssim 0.63$ (86 objects). Spectra displaying absorption and continuum properties consistent with the mean stellar template were classified as stars (8 objects). Spectra that could not be classified (32 objects) fell into two groups: low-S/N spectra displaying no identifiable spectral signature and spectra displaying significant contamination from extraneous LED light or instrumental defects. Table 6 summarises the number of objects identified in each class for the 1998/09/16–17 2dF observations. Examples of classifications from each category are shown in Figure 8. The stellar contamination of the early-type galaxy sample is $\simeq 2\%$.

The sample of early-type galaxy spectra was subdivided to account for variations in data quality. Sample A (433 objects) contains all spectra with reliable continuum shapes. This excludes spectra from MT field 5 observed using CCD2 which display evidence of contamination by LED light. Sample A is used to determine continuum-dependent properties, i.e. the composite spectrum and 4000Å break indices. Sample B (485 objects) contains all spectra for which reliable redshifts could be determined.

3.5 Redshift determination

The position of the cross-correlation peak indicates the galaxy redshift. However, for 19 spectra, with $R \lesssim 6$, the cross-correlation method proved unsatisfactory, due either to weak absorption features or residuals due to bad pixels, cosmic-rays or night-sky residuals at the wavelengths of major absorption features (e.g. CaII (H+K), G-band and

[‡] The R-value describes the ratio of the cross-correlation peak height to (twice) the antisymmetric noise component and offers an estimate of the significance of the cross-correlation peak.

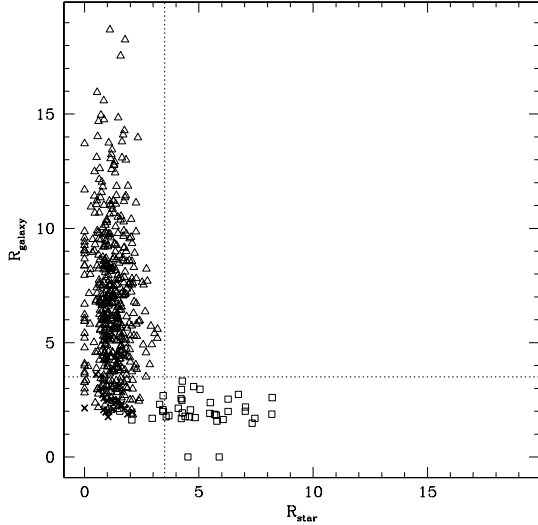


Figure 7. R-values for the 525 2dF spectra derived from cross-correlation with stellar (X-axis) and galaxy (Y-axis) templates using *xcsao*. Adopted spectroscopic classifications are indicated for early-type galaxies (open triangles), stars (open squares) and unclassified spectra (crosses).

Mgb). These objects were assigned redshifts interactively using the 4000Å break and less prominent absorption features (e.g. H δ , H β and Fe lines).

As a check of the redshift assignments, each spectrum was de-redshifted to the rest-frame and the wavelength interval 3500–4500Å plotted. This permitted a rapid visual check of the redshift of each spectrum by noting the position of the strong CaII H+K absorption plus the 4000Å break feature.

Errors in the cross-correlation velocity returned by the IRAF routine *xcsao* are computed based on the fitted peak height and antisymmetric noise associated with the identified cross-correlation peak (Tonry and Davis 1979; Heavens 1993). As expected with moderate to low S/N data, the error in the returned velocity estimate is a strong function of galaxy spectral S/N (Figure 10). The base level of error is $\sim 35 \text{ km s}^{-1}$ yet the sample displays a “tail” of velocity errors $\lesssim 200 \text{ km s}^{-1}$ at $S/N \lesssim 10$.

Some variation in redshift completeness as a function of apparent magnitude is expected. However, there is no evidence for any differences in the fractional redshift completeness rate for galaxies observed on different nights or in the two different fields. Therefore, a redshift incompleteness correction as a function of apparent magnitude only is derived. The number of the 525 early-type galaxy targets identified as stars (8) constitutes a very small percentage, $\simeq 2\%$, of the total and the majority of the 32 objects that remain unidentified are almost certainly early-type galaxies. Assuming this to be the case, Figure 9 displays redshift completeness as a function of apparent r -magnitude for the sample of 517 objects comprising the early-type galaxies and unidentified spectra. The fractional completeness is extremely high (0.95) and shows only a weak dependence on apparent magnitude. In fact, the low S/N and LED-contaminated spectra making up the unidentified objects

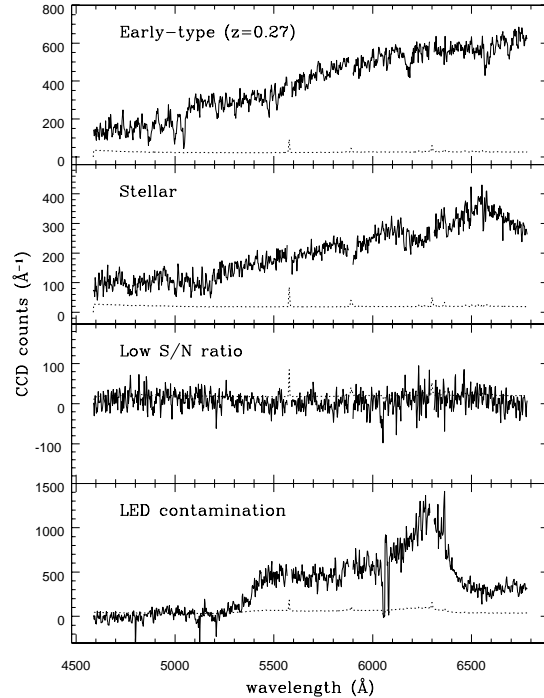


Figure 8. Example spectra drawn from each spectral class. The dotted line indicates the 1σ noise level in each case.

result primarily from factors such as low fibre throughput, astrometric errors, and fibre placement errors, unrelated to the target magnitudes.

3.6 Flux calibration

The homogeneous nature of the target galaxy population enables a highly effective “bootstrap” procedure to be employed to determine a relative flux scale. The procedure is based on the comparison of each object classified as an early-type galaxy to a reference early-type galaxy template (Kinney et al. 1996). The template spectrum was redshifted and resampled to provide a match to the observed-frame spectrum of each early-type galaxy. The template was then appropriately normalized and divided into the galaxy spectrum. The overall similarity of the resulting ~ 60 individual response functions per field+CCD confirmed the homogeneous nature of the galaxy population. The median response per pixel (i.e. wavelength) was calculated and a third-order cubic spline function fitted to produce a response function for each field+CCD combination.

The response function for each field+CCD was applied to all spectra observed with the respective field+CCD combination. The form of the response function accords well with expectations based on the properties of the atmospheric transmission, spectrograph grating efficiency and CCD quantum efficiency. However, an independent test to show that the reference template is indeed appropriate is desirable. The inclusion of the 33 stellar objects with colours consistent with M-stars scattered from the stellar locus (Figure 2) allows such a test to be performed. A composite stellar spectrum was generated from the 33 individual re-

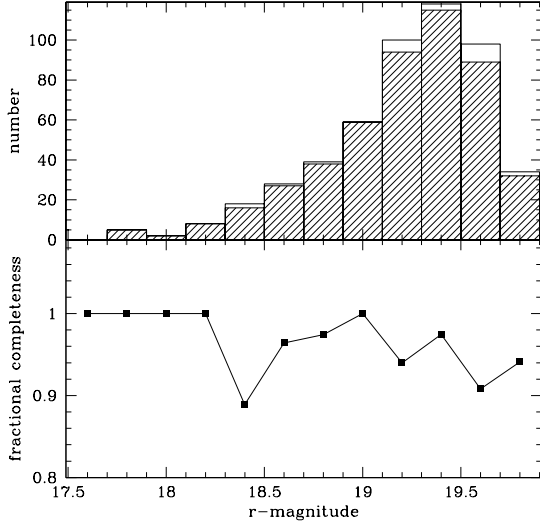


Figure 9. Top panel: Number–magnitude histogram. The open histogram indicates the number of objects in each apparent magnitude bin. The shaded histogram indicates the number of objects allocated a redshift. Bottom panel: Fractional redshift completeness versus apparent r –magnitude.

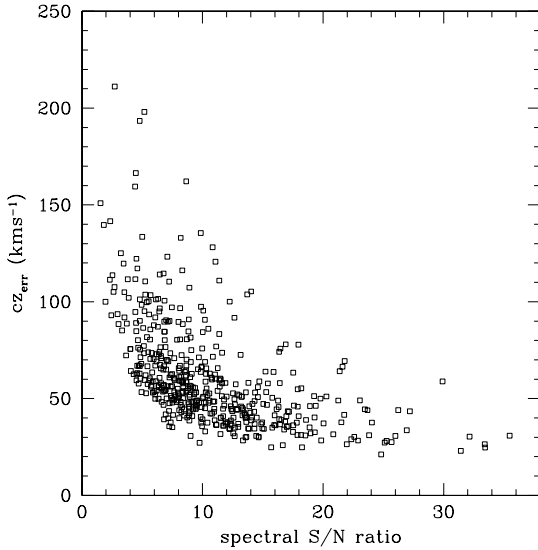


Figure 10. Galaxy redshift velocity error as a function of spectral S/N.

response function–corrected spectra. Figure 6 shows the “flux–corrected” mean stellar spectrum together with a reference M2V spectrum. The spectral type has been chosen to produce the best match to the absorption features, not to optimise the match of the continua. The agreement in the shape of the continua over intermediate and large scales indicates that the bootstrap procedure based on the use of a reference early–type galaxy template produces a relative flux scale accurate to $\sim 10\%$. Such an accuracy is typical for observations using narrow slits over wavelength intervals of $\sim 2000 \text{ \AA}$ and can be achieved for the 2dF observations because of the extremely homogeneous nature of the galaxy

target spectra and their similarity to the $z \sim 0$ early–type galaxy template.

An absolute flux zero–point for each spectrum can be derived using the apparent magnitudes after allowing for the fraction of light from the galaxy, modeled as a de Vaucouleurs (1948) surface brightness distribution with half–light radius $1''$, entering the $2''$ diameter fibres in the seeing conditions appropriate to the 2dF observations. The conversion factor between the UKST broad–band i –magnitudes and the flux present in the spectral interval $4800\text{--}6600 \text{ \AA}$ was determined from a suitably redshifted version of the Kinney early–type galaxy template, together with the UKST i –band filter and photographic emulsion response functions.

4 STATISTICAL PROPERTIES OF THE SAMPLE

4.1 The composite early–type galaxy spectrum

The early–type galaxy sample is sufficiently homogeneous that the properties of the composite spectrum are potentially of considerable interest. To generate a composite spectrum, all early–type galaxy spectra in Sample A (Section 3.4) were de–redshifted and resampled, using 1.5 \AA pixels, onto the rest–frame wavelength interval $2900\text{--}5405 \text{ \AA}$. An associated quality array specified the location of bad CCD pixels, missing data and residual signatures associated with prominent night–sky emission features. Wavelengths so flagged in the quality array were not included in the generation of the composite.

Prior to combination, each spectrum was normalised to a uniform mean count value of unity over the rest–frame wavelength interval $3670\text{--}4180 \text{ \AA}$, the interval common to all spectra. An initial composite spectrum and associated 1σ noise estimate was calculated according to:

$$\bar{R}_j = \frac{1}{n_{\text{spec}}} \sum_{i=1}^{n_i} k_i R_{ij}, \quad (1)$$

$$\bar{N}_j = \left[\frac{1}{n_{\text{spec}}} \sum_{i=1}^{n_i} (k_i N_{ij})^2 \right]^{\frac{1}{2}}, \quad (2)$$

where \bar{R}_j is the composite spectrum over pixels $j = 1, n_{\text{spec}}$. R_{ij} is the j th pixel of the i th spectrum. k_i is the normalisation constant applied to each spectrum. \bar{N}_j and N_{ij} are the corresponding 1σ noise values per pixel.

The initial estimate of the composite spectrum was used as a template to identify any remaining bad pixels not included in the quality arrays (e.g. poorly removed cosmic rays). Each spectrum was divided by a suitably scaled version of the composite spectrum to generate an exact transformation between the spectra. The transformation array was median–filtered with a 31–pixel window ($\sim 70 \text{ \AA}$) to remove positive and negative deviations on wavelength scales $\lesssim 30 \text{ \AA}$ yet preserve large–scale continuum variations. The composite was then scaled using the median–filtered transformation array and subtracted from the individual spectrum to produce a residual spectrum. Pixels deviating by $>5\sigma$ from zero in each residual spectrum were added to the quality array. Very few pixels ($\lesssim 5$) were rejected from individual spectra via this step. To investigate the homogeneity

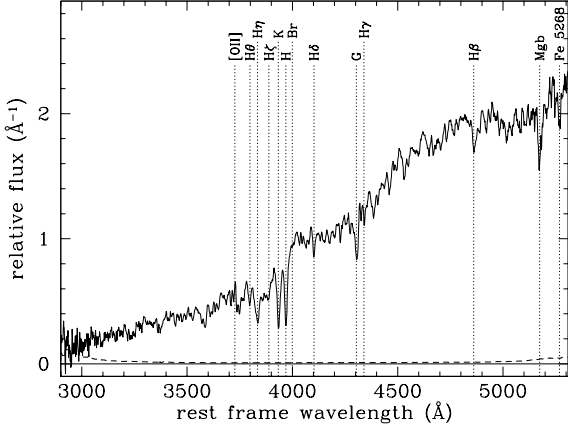


Figure 11. The composite spectrum resulting from four iterations of χ^2 rejection algorithm. The dashed line indicates the associated 1σ noise array. The solid horizontal line indicates the zero relative flux level. Prominent rest-frame absorption features are indicated by vertical dotted lines.

of the sample quantitatively, the normalised χ^2 statistic was calculated for each individual spectrum and the scaled composite over the full rest-frame wavelength interval:

$$\chi_i^2 = \frac{1}{n_{pix}} \sum_{j=1}^{n_{pix}} \frac{(R_{ij} - \bar{R}_j/k_i)^2}{N_{ij}^2}. \quad (3)$$

Given the goal of obtaining a composite spectrum representative of the homogeneous element of the sample, objects with $\chi^2 > 3.0$ were excluded from the calculation of the composite. This procedure was repeated four times to produce the final composite. The number of spectra rejected at each iteration was 49, 4, 2, 0 confirming both the stability of the procedure and the homogeneity of the bulk, $\sim 90\%$, of the galaxy spectra. The resulting composite spectrum is shown in Figure 11. Figure 12 displays the final χ^2 histogram of all spectra contributing to the composite. The narrow distribution of values with a peak at $\chi^2 = 1.2$ confirms the very high degree of homogeneity of the majority of spectra in the early-type galaxy sample.

Figure 13 indicates that the composite early-type galaxy spectrum is virtually indistinguishable from the Kinney early-type galaxy template. The detailed resemblance between the two spectra is not a result of the flux calibration procedure (Section 3.6), which effectively matches the two spectra only over wavelength scales $\gtrsim 1000\text{\AA}$. The excellent match between the composite stellar spectrum and a template of spectral type M2V (Figure 5) confirms the similarity of the composite galaxy spectra to the Kinney template is not a result of the bootstrap calibration procedure. A quantitative comparison of the spectroscopic properties of the early-type galaxy sample and the Kinney template will be presented in Paper II (Willis et al. 2001, in preparation).

4.2 The variation in spectroscopic properties

The $\sim 10\%$ (55 objects) of spectra excluded by the χ^2 criterion in the generation of the composite spectrum constitute themselves a relatively homogeneous population with

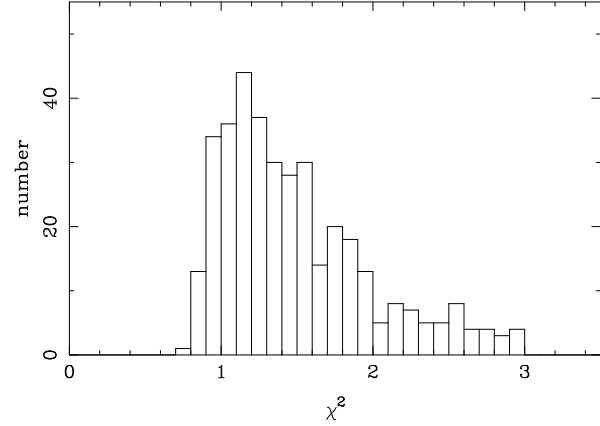


Figure 12. Histogram of χ^2 values after four iterations of the rejection algorithm.

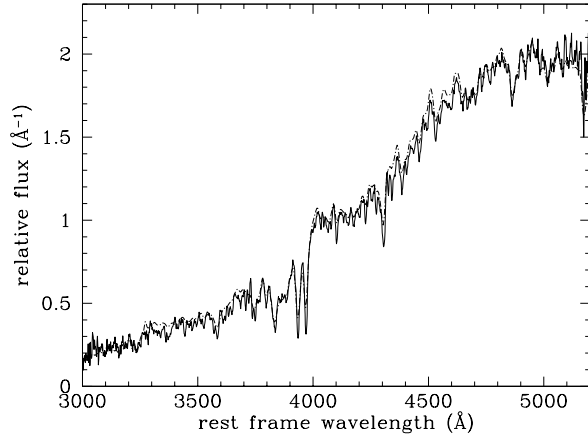


Figure 13. Comparison of the composite early-type galaxy spectrum (solid line) to the Kinney template (dashed line).

objects occurring uniformly over all fields and among all fibres within fields. Comparison of the composite spectrum with the mean of the 55 excluded spectra (Figure 14) confirms that the spectra of the excluded objects are also early-type galaxies but with a slightly bluer continuum slope and marginally weaker absorption lines. Do these subtle differences reflect intrinsic differences in the spectral energy distributions among the target population or could they arise from limitations in the observations or reductions?

The dominant uncertainty in the overall shape of the individual spectra is the uncertainty associated with the vertical normalisation and shape of the sky residual. Examination of the absorption line properties and their relation to the variation in the shapes of the spectra offers the prospect of discriminating between instrumental and intrinsic explanations for the variation in spectroscopic properties.

Figure 15 shows the distribution of absorption line strengths for all 433 spectra in Sample A with objects included in (378 objects) and excluded from (55 objects) the composite identified separately. The top left panel shows absorption line strength index versus χ^2 (at the final iteration of the composite spectrum calculation). The absorption

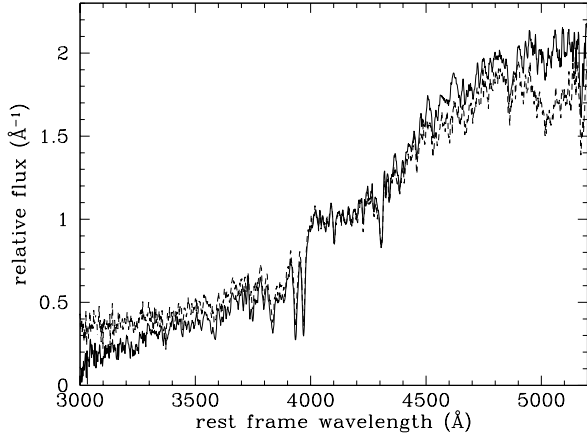


Figure 14. The composite spectrum (solid line) and the mean spectrum of the 55 excluded spectra (dashed line).

line strength index is the ratio of the combined absorption line strength of the most prominent absorption features in a spectrum to the combined absorption line strength in the composite spectrum. A value of unity indicates the strengths are the same and an index greater/less than unity indicates the line strength is greater/less than in the composite spectrum (see Appendix for an expanded discussion). The top right panel of Figure 15 shows the strength of the 4000Å break feature (D4000) in each early-type galaxy spectrum. This index is the ratio of the mean flux (rejecting outliers) over the wavelength range (4030–4180Å) to that in the wavelength range 3750–3900Å. More positive values of D4000 indicate a larger continuum discontinuity at 4000Å and vice versa.

The predicted variation in absorption line and 4000Å break indices due to the 2% uncertainty in sky-subtraction was obtained via simulations based on the composite spectrum. A series of spectral templates corresponding to the composite spectrum observed at S/N of 2 to 30, spanning the distribution in the observed sample, were generated. An additional spectral component, corresponding to a 2σ error in sky-subtraction was then added, or subtracted. The absorption line strength and D4000 indices were calculated for the simulated spectra and the results plotted as the dotted lines in Figure 15 (lower plots).

The observed spread in properties of spectra included in the calculation of the composite in Figure 15 is entirely consistent with the predictions based on the instrumental/reduction uncertainties. By contrast the 55 excluded spectra lie well away from the envelope defined by the $\pm 2\sigma$ errors in sky-subtraction and there is a marked excess of spectra that possess weaker absorption and shallower D4000 breaks. Their distribution in Figure 15 does not suggest they represent the tail of the distribution describing the bulk of the galaxy spectra. The trend for spectra with high S/N to be excluded from the composite when they possess absorption line strength and D4000 indices indicating only small differences from the mean arises due to the nature of the threshold χ^2 criterion.

Thus, examination of the inter-relation of spectroscopic properties and the effects of instrumental/reduction uncertainties suggests the sample of excluded spectra represent a

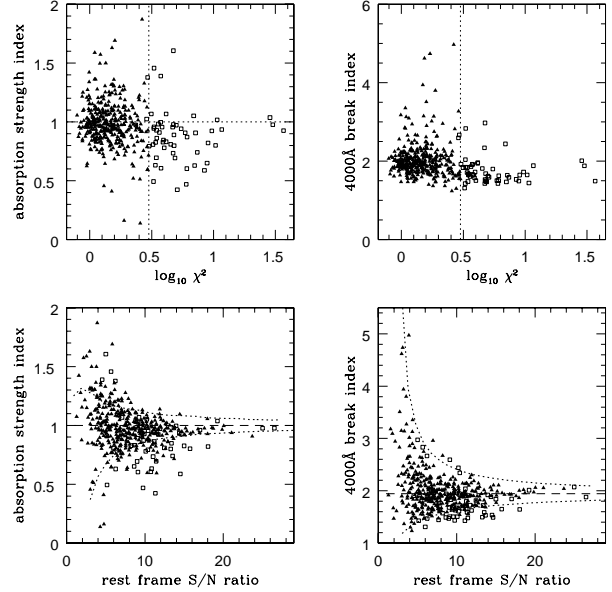


Figure 15. Continuum and absorption line properties of the early-type galaxy sample. Top left: Absorption line strength index versus $\log_{10} \chi^2$. The vertical dotted line indicates $\chi^2 = 3$. The horizontal dotted line indicates absorption line strength index = 1. Top right: 4000Å break index versus $\log_{10} \chi^2$. Bottom left: Absorption line strength index versus spectrum S/N. Bottom right: 4000Å break index versus spectrum S/N. Dotted lines in the bottom panels represent the 2σ error in the parameters associated with typical uncertainties in sky-subtraction. The central dashed lines show the index associated with the composite spectrum.

sub-sample of objects with bluer continua and weaker absorption features. Support for this conclusion is offered by the distribution of $b_j - or$ colours for the two samples of objects (Figure 16). An increasing fraction of objects with bluer observed $b_j - or$ colours is made up of objects excluded from the composite spectrum. A Kolmogorov–Smirnov test indicates that the two samples differ at the 92% confidence level. Taken alone, the increasing incidence of blue $b_j - or$ colours among the sample of spectra excluded from the composite is not significant. However, the result, when combined with the (completely independent) differences observed in the strength of the D4000 index from the spectra, supports the identification of the group of spectra excluded from the composite as possessing small but distinct differences in their spectral energy distributions compared to the composite spectrum.

In summary, $\sim 90\%$ of the sample possess spectra essentially indistinguishable from a redshift $z = 0$ early-type galaxy spectral energy distribution. Some 10% of the sample also possess spectra very similar to a $z = 0$ early-type galaxy spectrum but absorption line strengths are weaker by $\sim 20\%$ and the spectra are bluer by $\sim 25\%$ across the 4000 Å-break. The significance of this sub-population in the sample is discussed in Paper II (Willis et al. 2001, in preparation).

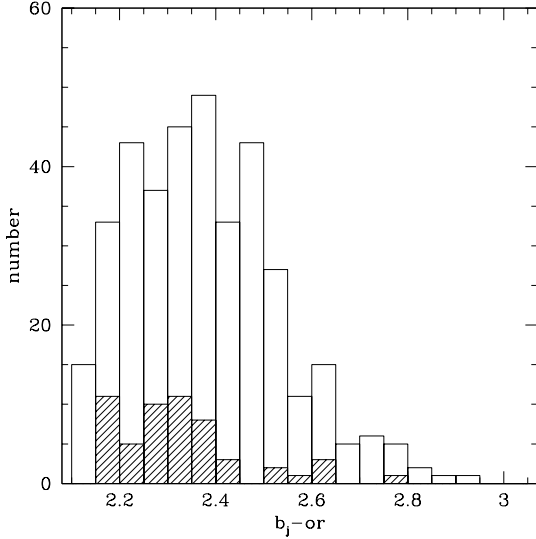


Figure 16. $b_j - or$ histograms of spectra included (unfilled) and excluded (filled) from the composite.

4.3 [OII] 3727 emission

Evidence for the presence of ongoing star formation or active galactic nuclei in the galaxies was sought via a search for [OII] 3727 emission in the “continuum subtracted” spectra of the galaxies. One goal of the project is to identify the presence of emission lines, due to background lensed sources, appearing at arbitrary wavelengths in the spectra of the galaxies. As a consequence, the continuum-subtraction algorithm employed was designed to remove both the continuum and absorption-line signature of the early-type galaxy over the full extent of the spectrum, leaving only potential emission lines. The composite galaxy spectrum (Section 4.1) provides a natural template for removal of the galaxy continuum and absorption line signature. However, weak [OII] 3727 emission is visible in the composite spectrum. Thus, the wavelength region 3720–3734Å was replaced by the corresponding region of the Kinney et al. (1996) early-type galaxy SED, suitably scaled to match the composite spectrum. Each individual galaxy spectrum was then divided by a suitably redshifted version of the modified composite spectrum. The resulting transformation array was median filtered, using a 31-pixel window ($\sim 70\text{\AA}$), in order to remove small scale features (which might include emission lines). The modified composite spectrum was then scaled using the median-filtered transformation array and subtracted from the galaxy spectrum.

This procedure proved extremely effective in removing the continuum signature of the galaxies but residual signal due to variations in the strength of absorption lines from galaxy to galaxy was still evident. An absorption line template, based on the presence of absorption features visible in the composite spectrum (Table A1), was generated. A least-squares procedure was then employed to determine the fractional scaling of the absorption line template that, when subtracted from each residual galaxy spectrum, minimised the absorption line signal (Appendix). The continuum and absorption line subtraction procedures applied to each galaxy spectrum produced a residual spectrum with

zero mean flux and deviations about zero due to noise plus excursions from any emission lines present. The noise properties are consistent with the Poisson noise per pixel determined by propagating the photon statistics of the original exposures through the reduction and analysis pipeline.

Emission lines could then be identified in the residual spectra using standard matched-filter techniques (e.g. Hewett et al. 1985). A Gaussian filter of 10\AA FWHM, truncated at 4 FWHM, was employed as the line template (chosen to be sensitive to the range of [OII] 3727 FWHM anticipated from the sample of luminous early-type galaxies given the instrumental resolution of the spectrograph). Cross-correlation of the template with the residual galaxy spectra produced, for each wavelength increment, a noise-weighted S/N quantifying the significance of any emission feature, a χ^2 -value describing the match to the shape of the Gaussian template and a vertical scaling for the template, from which the line flux and equivalent width may be calculated.

The search for [OII] 3727 emission was undertaken over the rest-frame wavelength interval $3717\text{\AA} < \lambda < 3737\text{\AA}$ while the two immediately adjacent 20\AA intervals provided an empirical control region. After some experimentation, candidate emission features were selected to possess $S/N \geq 3.5$ and $\chi^2 \leq 2.0$. The central wavelengths, FWHM and flux in the candidate lines were then calculated via a least squares fit of a three-parameter Gaussian profile to the data. Properties of the 104 emission lines selected at $S/N \geq 3.5$ and $\chi^2 \leq 2.0$ within the specified rest-frame wavelength interval, with fluxes derived from the three-parameter model fit, are included in Table 4.5. Figure 17 displays the number of detected emission-lines as a function of wavelength. The reality of the [OII] emission line detections is confirmed by the statistics of “detections” from the adjacent control regions, where, from a wavelength region twice that of the [OII] window, only 2 features satisfy the emission line selection parameters, i.e. ~ 1 of the 104 emission line detections is expected to be spurious.

4.4 The number-redshift distribution and absolute magnitude sampling

The number-redshift ($N(z)$) distribution of the 485 early-type galaxies from the 1998/05/16–17 sample is displayed in Figure 18. The galaxies span the redshift interval $0.25 \leq z \leq 0.63$ and the median redshift of the sample is $z_{med} = 0.391$. The observed $N(z)$ distribution is consistent with the predicted distribution generated by applying the survey selection criteria to an early-type galaxy population described by a representative spectral evolution model and luminosity function. A detailed discussion of the luminosity function and space density of the population is deferred until a later paper. However, for illustration, the predicted $N(z)$ for the sample employing the early-type galaxy luminosity function and evolution parameters of Pozzetti et al. (1996) in a cosmology specified by the parameters $\Omega = 0.3$, $\Lambda = 0.7$ and $H_0 = 70 \text{ km s}^{-1} \text{ Mpc}^{-1}$ is also shown in Figure 18.

Figure 19 shows the absolute V -band magnitude distribution versus redshift of the 485 early-type galaxies. Absolute magnitudes are expressed in the V -band as, at the median redshift of the sample, the UKST i -band samples the rest-frame V -band in each early-type galaxy. Absolute

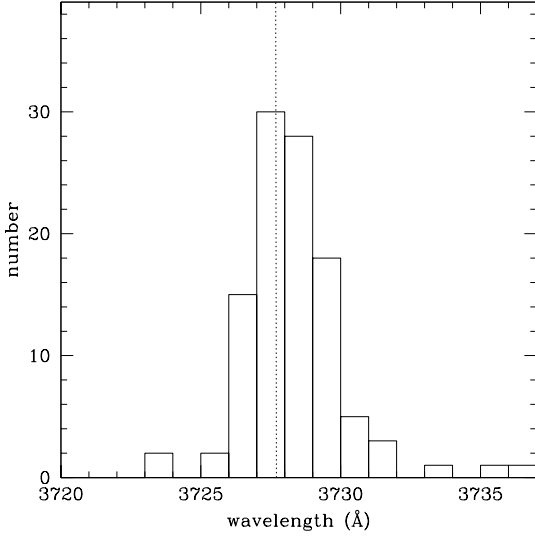


Figure 17. Wavelength centroid histogram for the 104 [OII] 3727 emission line detections. The vertical dashed line indicates 3727.7Å, the central wavelength of the [OII] doublet.

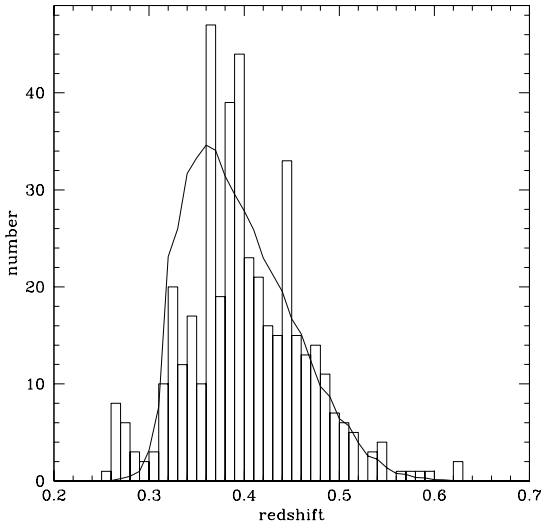


Figure 18. Number-redshift histogram of 485 early-type galaxies. The solid line indicates the number-redshift distribution predicted from applying the survey selection criteria to a simulated, passively evolving early-type galaxy population (see text).

V -band magnitudes were determined from apparent i -band magnitudes and redshifts according to

$$M_V(z) = m_i - 25 - 5 \log d_L(z) - e_i(z) - k_i(z) + (V - i)_0, (4)$$

where m_i is the apparent i -band magnitude of a given galaxy at a redshift z , $d_L(z)$ is the luminosity distance at a redshift z within the specified cosmological model, $e_i(z)$ parameterizes the luminosity evolution in the i -band, $k_i(z)$ is the k -correction for the i -band and $(V - i)_0$ is the $V - i$ colour for an early-type galaxy at $z = 0$. The dashed lines in Figure 19 indicate the absolute magnitude limits of the sample as a function of redshift defined by the i -band apparent

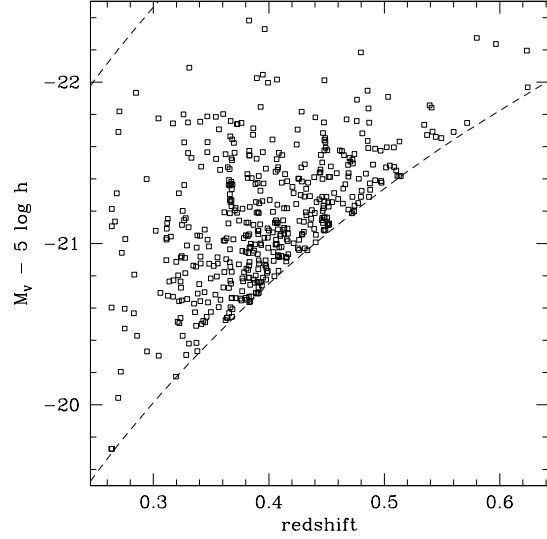


Figure 19. Absolute V -magnitude versus redshift of 485 early-type galaxies from the 1998/09/16–17 sample. The dashed lines indicate the apparent magnitude selection criteria $16.4 < i < 18.85$ transformed to rest-frame absolute V -magnitude according to equation 4.

magnitude selection criteria (Table 3), confirming that the majority of the early-type galaxy sample consists of highly-luminous galaxies ($-22.4 \lesssim M_V \lesssim -19.5$).

4.5 Redshift catalogue

Positions and magnitudes (Section 2), redshifts (Section 3.5) and [OII] 3727 emission line fluxes (Section 4.3) for the 485 galaxies observed during the 1998 September observations are presented in Table 4.5. The same information, aside from the emission line fluxes which are not available, for an additional 96 galaxies observed during 2dF runs prior to 1998 September are presented in Table 8. The complete redshift catalogue can be accessed via the Strasbourg astrophysical Data Center (CDS) located at the URL: <http://cdsweb.u-strasbg.fr/Cats.html>.

5 SUMMARY

Luminous, field early-type galaxies at cosmologically significant distances represent an important fraction of the population of normal galaxies that is almost entirely absent from the current generation of spectroscopic surveys. Identification of such galaxies out to redshifts of $z \sim 0.6$ can be readily achieved by applying a straightforward BRI broadband colour selection to photographic or CCD material that reaches only modest depth, $I \simeq 19$. Morphological information allows contaminating M dwarfs to be eliminated as candidates. However, for magnitudes $17 \leq I \leq 19$, and given photometric precision of $\lesssim 0.15$ mag, the number of galaxies greatly exceeds the number of stellar objects and stellar contamination is not a significant limitation in compiling galaxy samples. The key requirement for the assembly of a large sample of such galaxies is sky coverage as the surface density of objects to $I < 19.0$ is $< 100 \text{ deg}^{-2}$.

Landscape table to go here.

Table 7.

Table 8. Spectroscopic catalogue of 96 early-type galaxies based on pre-1998 September 2dF observations.

Galaxy	RA ^a (hh:mm:ss.ss)	Dec. (dd:mm:ss.s)	b_j	or	i	error(b_j)	error(or)	error(i)	z	cz_{err}^b (kms ⁻¹)
G1344m0020	13:44:55.61	-00:20:16.0	20.94	18.86	18.38	0.11	0.07	0.11	0.417	70
G1343m0023	13:43:31.45	-00:23:57.6	19.78	18.18	17.48	0.07	0.05	0.06	0.330	51
G1342m0027	13:42:44.75	-00:27:32.3	20.16	18.86	18.00	0.09	0.07	0.09	0.327	128
G1345m0019	13:45:00.77	-00:19:54.4	20.92	19.13	18.45	0.12	0.08	0.11	0.382	81
G1342m0026	13:42:37.78	-00:26:53.6	20.99	19.63	18.68	0.15	0.10	0.13	0.421	0
G1342m0021	13:42:59.67	-00:21:10.5	20.73	18.76	17.95	0.12	0.07	0.08	0.380	77
G1342m0030	13:42:39.99	-00:30:51.8	20.07	18.59	17.68	0.09	0.06	0.07	0.326	91
G1342m0038	13:42:05.46	-00:38:29.0	20.65	18.74	18.16	0.10	0.07	0.10	0.379	81
G1343m0043	13:43:11.57	-00:43:29.8	20.74	19.09	18.34	0.12	0.08	0.11	0.401	147
G1342m0044	13:42:27.18	-00:44:19.6	20.78	19.00	18.41	0.11	0.08	0.11	0.381	86
G1342m0019	13:42:05.73	-00:19:07.7	20.05	18.57	17.81	0.08	0.06	0.08	0.329	43
G1342m0100	13:42:56.40	-01:00:22.2	21.25	19.36	18.61	0.16	0.09	0.12	0.386	85
G1342m0014	13:42:57.05	-00:14:24.1	21.12	19.04	18.25	0.15	0.08	0.10	0.396	71
G1341m0050	13:41:56.26	-00:50:43.8	20.93	19.42	18.66	0.13	0.09	0.13	0.345	121
G1342m0103	13:42:26.40	-01:03:33.5	20.44	18.90	18.00	0.10	0.07	0.09	0.391	64
G1341m0019	13:41:03.63	-00:19:42.3	20.58	19.17	18.38	0.11	0.08	0.11	0.340	74
G1341m0023	13:41:13.76	-00:23:08.5	20.53	19.21	18.26	0.11	0.08	0.10	0.338	46
G1340m0108	13:40:58.38	-01:08:39.2	19.10	17.71	16.87	0.05	0.04	0.05	0.294	68
G1341m0037	13:41:11.69	-00:37:05.1	20.99	19.06	18.26	0.14	0.08	0.10	0.356	67
G1341m0058	13:41:21.72	-00:58:50.4	20.94	19.03	18.45	0.12	0.08	0.11	0.384	55
G1340m0101	13:40:52.86	-01:01:55.7	21.13	19.32	18.65	0.14	0.09	0.13	0.416	150
G1340m0058	13:40:41.52	-00:58:08.7	21.06	19.34	18.62	0.14	0.09	0.12	0.355	134

^a Positions are J2000.0.

^b A zero value indicates redshift assigned visually.

Using APM scans of UKST b_j , or and i photographic plates we have compiled a photometric catalogue of 9599 candidate galaxies, magnitudes $m_i \leq 18.95$, over 220 deg^2 in seven UKST fields. From the results of spectroscopic observations the contamination by stellar objects, M dwarfs, is only $\sim 2\%$.

Spectroscopic observations of a sample of 581 galaxies from the photometric catalogue are presented. The galaxies span the redshift interval $0.25 \leq z \leq 0.63$ with absolute magnitudes $-22.4 \leq M_V \leq -19.5$. The absorption and emission line properties of the sample are parameterised and a high signal-to-noise ratio composite spectrum is constructed. The galaxy spectra display very similar spectral energy distributions, including a narrow range of absorption line strengths and 4000\AA -break indices. Comparison of the spectra with that of a local early-type galaxy template demonstrates that the rest-frame optical spectra of the galaxies in the sample are consistent with an old, passively evolving stellar population with little evidence of recent star-formation.

The sample represents a unique resource and will form the basis for investigations in the fields of gravitational lensing, galaxy evolution as a function of environment and the evolution of large scale structure to be presented in forthcoming papers.

ACKNOWLEDGMENTS

The staff of the Anglo-Australian Observatory provided invaluable assistance during the acquisition of the spectroscopic observations. We are grateful for the active longterm support of the United Kingdom Schmidt Telescope Unit

and the staff of the Automated Plate Measuring facility. The Isaac Newton Telescope is operated on the island of La Palma by the Isaac Newton Group in the Spanish Observatorio del Roque de los Muchachos of the Instituto de Astrofísica de Canarias. JPW acknowledges the support of a PPARC research studentship and financial support from IoA, Cambridge. The project would not have been possible without the data and analysis facilities provided by the Starlink Project which is run by CCLRC on behalf of PPARC.

REFERENCES

- Bailey, J., Glazebrook, K., 1999, 2dF User Manual, Anglo-Australian Observatory, Sydney
- Colless, M. M., 1999, Phil. Trans. Roy. Soc. Lond. A, 357, 105
- Crampton, D., Le Fevre, O., Lilly, S. J., Hammer, F., 1995 ApJ, 455, 96
- de Vaucouleurs, G., 1948, Ann. Astrophys, 11, 247
- Ellis, R.S., 1997, ARA&A, 35, 389
- Hamilton, D., 1985, ApJ, 297, 371
- Heavens, A.F., 1993, MNRAS, 263, 735
- Hewett, P.C., Irwin, M.J., Bunclark, P., Bridgeland, M.T., Kibblewhite, E.J., He, X.T., Smith, M.G., 1985, MNRAS, 231, 971
- Hewett, P.C., Warren, S.J., Willis, J.P., Bland-Hawthorn, J.B., Lewis, G.F., 2000, in van Breugel W., Bland-Hawthorn J.B., eds, ASP Conf. Ser. Vol. 195, Imaging the Universe in Three Dimensions: Astrophysics with Advanced Multi-Wavelength Imaging Devices. Astron. Soc. Pac., San Francisco, p. 94
- Høg, E., Fabricius, C., Makarov, V. V., Bastian, U., Schwekendiek, P., Wicenec, A., Urban, S., Corbin, T., & Wycoff, G. 2000, A&A, 357, 367
- Kinney, A.L., Calzetti, D., Bohlin, R.C., McQuade, K., Storchi-Bergmann, T., Schmitt, H.R., 1996, ApJ, 467, 38

Table A1. Absorption features identified in the composite spectrum.

Feature	Wavelength (Å)	Interval (Å)
H κ	3752.2	3744.5–3753.5
H η	3837.5	3822.5–3896.0
H ζ	3891.2	3822.5–3896.0
CaII K	3933.4	3924.5–3952.0
CaII H	3969.2	3952.5–3980.0
H δ	4102.8	4097.0–4109.0
G–band	4303.4	4295.0–4316.0
Fe4383	4383.0	4380.5–4392.5
Ca4455	4455.0	4455.5–4464.5
Fe4531	4531.0	4526.0–4536.5
H β	4861.3	4853.0–4880.0
Fe4890	4890.0	4884.5–4895.0
blend	4921.0	4917.5–4925.0
Fe5015	5015.0	5012.0–5024.0
Mgb	5174.0	5147.0–5196.5
blend	5206.0	5201.0–5214.5
Fe5268	5268.0	5256.5–5280.5
Fe5335	5335.0	5324.0–5346.5

- Lissandrini, C., Cristiani, S., La Franca, F., 1994, *PASP*, 106, 1157
- Maddox, S.J., Efstathiou, G.P., Sutherland, W.J., 1990, *MNRAS*, 246, 433
- Pickles, A.J., 1998, *PASP*, 110, 863
- Pozzetti, L., Bruzual, G., Zamorani, G., 1996, *MNRAS*, 281, 953
- Tonry, J., Davis, M., 1979, *AJ*, 84, 1511
- Turnshek, D.E., Turnshek, D.A., Craine, E.R., 1995, *An atlas of digital spectra of cool stars*, Tucson
- van Dokkum, P.G., Franx, M., Kelson, D.D., Illingworth, G., Fisher, D., Frabican, D., 1998, *ApJ*, 500, 714
- Warren, S.J., Hewett, P.C., Irwin, M.J., Osmer, P.S., 1991, *ApJ*, 76, 1
- Wyse, R.F.G., Gilmore, G., 1992, *MNRAS*, 257, 1

APPENDIX A: ABSORPTION LINE STRENGTH

The 2dF spectra of the galaxy sample possess relatively low S/N and are of only intermediate, $\sim 4\text{\AA}$, resolution. Equivalent widths of individual absorption features are thus very uncertain. To provide a more reliable measure of absorption line strength for each galaxy an absorption line template was fitted to all prominent absorption features in each spectrum, thus maximising the S/N of a measurement of absorption line strength. The combined absorption line strength in a particular early-type galaxy spectrum is expressed as a fraction of the absorption line strength in the composite galaxy spectrum.

Rest-frame wavelength regions associated with significant absorption features were identified by selecting features in the composite galaxy spectrum displaying a flux decrement greater than 12.5% relative to the locally-determined continuum. Absorption features identified via this method are listed in Table A1 and are indicated in Figure A1.

To prepare the galaxy spectra for the absorption line strength measurement it is necessary to define a reliable continuum. Each early-type galaxy spectrum was divided by a suitably scaled and redshifted version of the composite galaxy spectrum to generate an exact transformation between the spectra. The transformation array was median-

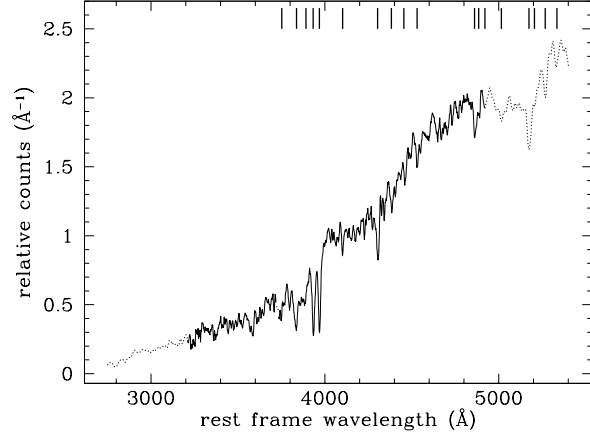


Figure A1. Composite early-type galaxy spectrum employed in absorption line analyses. The mean early-type galaxy spectrum is indicated by the solid line and the Kinney early-type template by the dotted line. Vertical solid lines mark the wavelength centres of absorption features listed in Table A1.

filtered with a 31-pixel window ($\sim 70\text{\AA}$) to remove positive and negative deviations on wavelength scales $\lesssim 30\text{\AA}$ yet preserve large-scale continuum variations. The composite spectrum was then scaled using the median-filtered transformation array to match each galaxy spectrum. Absorption line spectra for data and matched template spectra were generated by fitting and subtracting continuum profiles.

The absorption line strength measure for a galaxy is calculated from the scaling of the absorption line template to the galaxy's absorption line profile generated as described above. In the presence of random noise the most probable value of the scaling factor that matches the absorption line template to a galaxy's absorption line profile is obtained by minimising the weighted sum of the squared error residuals between the data and the template. If D_i is the data spectrum, P_i is the template absorption profile and σ_i is the 1σ noise per pixel, one then minimises the χ^2 expression $\chi^2 = \sum_i (D_i - kP_i)^2 / \sigma_i^2$ with respect to the scale factor k . The sum runs over the i pixels of the absorption line template. The value of the scale factor that minimises the sum is given by

$$k = \frac{\sum_i (D_i P_i) / \sigma_i^2}{\sum_i (P_i / \sigma_i)^2}. \quad (\text{A1})$$

Thus a scale factor of $k=1$ means that the line strength in a spectrum is equal to the line strength in the template whereas $k > 1$ means that the line strength is greater than the template, and vice versa.

This paper has been produced using the Royal Astronomical Society/Blackwell Science \LaTeX style file.

Table 7. Spectroscopic catalogue of 485 early-type galaxies based on 1998 September 2dF observations.

Galaxy	RA ^a (hh:mm:ss.ss)	Dec. (dd:mm:ss.s)	b_j	or	i	error(b_j)	error(or)	error(i)	z	cz_{err} ^b (kms ⁻¹)	$F_{[OII]}$ ^c	ID code ^d
G0149m3947	1:49:17.64	-39:47:01.1	21.80	19.38	18.67	0.17	0.09	0.13	0.382	0	1.19	1
G0148m3953	1:48:03.15	-39:53:34.6	20.89	18.66	17.85	0.10	0.06	0.09	0.312	38	0.00	1
G0146m3950	1:46:46.86	-39:50:17.3	21.78	19.63	18.64	0.17	0.10	0.13	0.367	76	1.72	1
G0149m3940	1:49:07.09	-39:40:15.2	21.55	19.31	18.43	0.15	0.09	0.12	0.454	58	1.77	1
G0149m3935	1:49:29.54	-39:35:41.2	21.62	19.24	18.50	0.16	0.08	0.12	0.453	53	0.00	1
G0148m3934	1:48:19.40	-39:34:36.3	21.92	19.43	18.78	0.19	0.09	0.14	0.451	66	0.00	1
G0149m3913	1:49:56.81	-39:13:23.2	21.73	19.47	18.71	0.17	0.09	0.14	0.404	67	0.00	1
G0148m3937	1:48:07.84	-39:37:45.8	21.75	19.36	18.80	0.17	0.09	0.14	0.451	53	5.17	1
G0149m3921	1:49:29.67	-39:21:20.5	21.75	19.36	18.65	0.17	0.09	0.13	0.404	80	0.00	1
G0148m3937	1:48:27.87	-39:37:30.8	21.39	19.01	18.39	0.14	0.07	0.12	0.487	86	0.00	1
G0148m3926	1:48:09.81	-39:26:47.6	21.87	19.50	18.51	0.18	0.09	0.12	0.366	58	0.00	1
G0148m3910	1:48:22.31	-39:10:58.7	21.35	19.17	18.26	0.14	0.08	0.11	0.449	90	0.00	1
G0148m3915	1:48:17.53	-39:15:18.3	21.80	19.28	18.32	0.17	0.09	0.11	0.476	53	2.78	1
G0147m3857	1:47:22.39	-38:57:55.9	22.05	19.70	18.65	0.20	0.11	0.13	0.484	111	0.00	1
G0146m3928	1:46:52.78	-39:28:51.2	21.05	18.69	17.73	0.12	0.06	0.08	0.367	44	0.00	1
G0145m3930	1:45:48.78	-39:30:56.8	21.70	19.47	18.60	0.17	0.09	0.13	0.323	58	0.00	1
G0145m3858	1:45:23.57	-38:58:21.2	21.17	18.79	18.14	0.12	0.07	0.10	0.320	48	0.00	1
G0146m3852	1:46:03.48	-38:52:57.0	21.90	19.55	18.55	0.19	0.10	0.13	0.541	67	0.00	1
G0144m3858	1:44:44.64	-38:58:28.6	21.87	19.43	18.67	0.18	0.09	0.13	0.358	52	0.00	1
G0144m3907	1:44:37.56	-39:07:50.8	22.05	19.64	18.82	0.20	0.10	0.14	0.376	67	0.00	1
G0144m3858	1:44:12.16	-38:58:57.9	22.05	19.67	18.79	0.20	0.10	0.14	0.624	125	0.00	1
G0145m3921	1:45:12.19	-39:21:08.1	21.86	19.58	18.74	0.18	0.10	0.14	0.545	56	0.00	1
G0142m3908	1:42:27.21	-39:08:17.9	20.79	18.62	17.77	0.10	0.06	0.08	0.363	48	4.24	1
G0142m3907	1:42:33.35	-39:07:41.3	21.45	19.25	18.41	0.14	0.08	0.12	0.356	50	0.00	1

^a Positions are J2000.0.

^b A zero value indicates redshift assigned visually.

^c $\times 10^{-17}$ ergs s⁻¹ cm⁻²

^d 1 – early-type galaxy, 0 – early-type galaxy with blue continuum and weaker absorption lines, -1 – early-type galaxy taken from field MTF5 CCD2 (possible LED contamination).